2018

Hollow Core Fiber Based Interferometer for High Temperature (1000 °C) Measurement

Dejun Liu
Technological University Dublin, dejun.liu@tudublin.ie

Qiang Wu
Technological University Dublin, qiang.wu@tudublin.ie

Chao Mei
Beijing University of Posts and Telecommunications

See next page for additional authors

Recommended Citation

Liu, D., Wu, Q. & Mei, C. (2018). Hollow core fiber based interferometer for high temperature (1000 °C) measurement, *Journal of Lightwave Technology*, vol. 36, no. 9. 10.1109/JLT.2017.2784544

This article has been accepted for publication in a future issue of this journal, but has not been fully edited. Content may change prior to final publication. Citation information: DOI 10.1109/JLT.2017.2784544, Journal of Lightwave Technology

Hollow Core Fiber Based Interferometer for High Temperature (1000 °C) Measurement

Dejun Liu, Qiang Wu, Chao Mei, Jinhui Yuan, Xiangjun Xin, Arun Kumar Mallik, Fangfang Wei, Wei Han, Rahul Kumar, Chongxiu Yu, Shengpeng Wan, Xingdao He, Bo Liu, Gang-Ding Peng, Yuliya Semenova, and Gerald Farrell

***Abstract*—A simple, cost effective high temperature sensor (up to 1000 °C) based on a hollow core fiber (HCF) structure is reported. It is configured by fusion splicing a short section of HCF with a length of few millimeters between two standard single mode fibers (SMF-28). Due to multiple beam interference introduced by the cladding of the HCF, periodic transmission dips with high spectral extinction ratio and high quality (Q) factor are excited. However, theoretical analysis shows that minor variations of the HCF cladding diameter may result in a significant decrease in the Q factor. Experimental results demonstrate that the position of periodic transmission dips are independent of the HCF length, but spectral Q factors and transmission power varies with different HCF lengths. A maximum Q factor of 3.3×10^4 has been demonstrated with large free spectral range of 23 nm and extinction ratio of 26 dB. Furthermore, the structure is proved to be an excellent high temperature sensor with advantages of high sensitivity (up to 33.4 pm/°C), wide working temperature range (from room temperature to 1000°C), high resolution, good stability, repeatability, relatively low strain sensitivity (0.46 pm/με), low cost and a simple and flexible fabrication process that offers a great potential for practical applications. A thorough theoretic analysis of the HCF based fiber structure has been proposed. The experimental results are demonstrated to be well matched with our simulation results.**

***Index Terms*—Temperature sensors, optical fiber sensors, optical spectroscopy, optical interferometry, optical fiber applications.**

Manuscript received XXXX; revised December XXXX; accepted XXXX. Date of publication XXXX; date of current version XXXX. This work was supported in part by DIT FIOSRAIGH 2012 (Dean of Graduate Students Award); in part by Open Fund of IPOC (BUPT); in part by Science Foundation Ireland (SFI/13/TIDA/B2707, SFI/13/ISCA/2845); and in part by the National Natural Science Foundation of China under grant No. 61465009. (D. Liu and Q. Wu contribute equally to this work.) (Corresponding author: Q. Wu and J. Yuan).

D. Liu, A. K. Mallik, F. Wei, W. Han, Y. Semenova, and G. Farrell are with the Photonics Research Centre, Dublin Institute of Technology, Kevin Street, Dublin 8, Ireland (email: dejun.liu@mydit.ie; d13125763@mydit.ie; fangfang.wei@mydit.ie; d14125980@mydit.ie; yuliya.semenova@dit.ie; gerald.farrell@dit.ie).

Q. Wu and R. Kumar are with the Department of Mathematics, Physics and Electrical Engineering, Northumbria University, Newcastle Upon Tyne, NE1 8ST, United Kingdom (email: qiang.wu@northumbria.ac.uk; rahul.kumar@northumbria.ac.uk). Q. Wu is also with the School of Physics & Optoelectronic Engineering, Nanjing University of Information Science & Technology, Nanjing 210044, China

B. Liu is with the School of Physics & Optoelectronic Engineering, Nanjing University of Information Science & Technology, Nanjing 210044, China (bo@nuist.edu.cn).

C. Mei, J. Yuan, X. Xin and C. Yu are with the Beijing University of Posts and Telecommunications, Beijing 100876, China (email: GY_mei@163.com; yuanjinhui81@163.com; xjxin@bupt.edu.cn; cxyu@bupt.edu.cn).

S. Wan and X. He are with the Jiangxi Engineering Laboratory for Optoelectronics Testing Technology, Nanchang Hangkong University, Nanchang 330063, China (email: sp_wan@163.com; xingdaohe@126.com).

G. Peng is with the School of Electrical Engineering & Telecommunications, University of New South Wales, Sydney 2052, NSW, Australia (g.peng@unsw.edu.au).

I. Introduction

Optical fiber sensors have been widely studied due to their well-known advantages such as miniature size, immunity to electromagnetic interference, a high resistance to corrosive environments, fast response and remote sensing capabilities, which gives them a great potential to be used in many applications including refractive index sensing, bio-chemical sensing, large civil structures structural health monitoring, and gas exploration [1-5]. Some of these applications require the sensors to have the ability to work at very high temperatures with good stability and accuracy. Previously reported optical fiber based temperature sensors can be mainly categorized into two types depending on the physical principle of sensor operation. One type is grating based temperature sensors while the other type are sensors whose operation is based on interferometry. Among these different types of temperature sensors, fiber Bragg grating (FBG) based temperature sensors are the most developed and reliable temperature sensors in real-life applications because of their unique advantages of high quality factor (Q factor, usually larger than 10^4) and multiplexing features [6]. However, the traditional Type I grating based FBG introduced by moderate UV exposures can be easily erased under high temperature, so it can only be used for relatively low temperature applications (usually below 200 °C). By utilizing an intensive UV laser source or femtosecond pulse duration infrared (fs-IR) laser source, other types of gratings can be inscribed. The working temperature of these kinds of grating sensors can be extended to over 1000 °C [7-9]. However, the fabrication process for such gratings is rather complicated and expensive [10]. Interferometer based temperature sensors, on the other hand, have the advantages of a relatively simple fabrication process, a much lower cost and can be fabricated for example by tapering or combining different optical fiber structures. Based on a variety of different fiber structure configurations, a number of interferometer based sensors have been proposed for high temperature sensing, such

This article has been accepted for publication in a future issue of this journal, but has not been fully edited. Content may change prior to final publication. Citation information: DOI 10.1109/JLT.2017.2784544, Journal of Lightwave Technology

as those based on multimode fibers, thin core fibers, microcavities, microchannels, twin core, multi core fibers, and photonic crystal fibers (PCF) [11-17]. Multimode and thin core fiber based temperature sensors show poor spectral Q factors and hence the temperature measurement accuracy is relatively low. Microcavity and microchannel based Fabry-Perot interferometer (FPI) temperature sensors could achieve higher Q factors but with extremely smaller channel spacing and hence narrow measurement range [18]. Besides, the fabrication of such microcavities or microchannels typically requires high cost equipment such as a femtosecond laser. PCF based temperature sensors have also attracted lot of interest recently, but they suffer from the disadvantages of large insertion loss, low fringe visibility and high cost.

Hollow core fiber (HCF) is attracting more and more research interest, for example, as a means to incorporate an air-gap microcavity in the HCF to form an FPI for sensing applications [19-21]. In FPI based sensors there is a need to very precisely control the size of the microcavity in the order of micrometers, as small variations in the cavity length will result in significant changes to the actual spectrum achieved by comparison to the intended spectrum. Moreover, most of the air gap FPI based temperature sensors have a very limited temperature sensitivity (~1 pm/°C) [22-24] and contamination from dust and other pollutants is a significant issue for the long term stability of the sensor, due to a structure that is typically open to the environment [11]. Recently, functionalized HCF based interferometer structures has been reported for use as a biosensor, a magnetic field sensor, a humidity sensor and a displacement sensor [25-28]. These reports demonstrated very useful applications of a HCF based interferometer, but to date there has been a lack of in-depth analysis of the structure.

In this article, we propose and investigate a single HCF (~30 μm inner diameter, ~126 μm outer diameter) based multiple beam interferometer for high temperature sensing, where a short section of HCF is fusion spliced between two traditional singlemode fibers (SMF28). The proposed structure demonstrates a high spectral extinction ratio (over 26 dB), high Q factor (3.3×10^4), wide working temperature range (up to 1000°C), a high temperature sensitivity of 34.3 pm/°C and a relatively low strain sensitivity of about 0.46 pm/με. The demonstrated sensor has the advantages of low cost and a simple and flexible fabrication process that offers a great potential for practical applications.

II. Theoretical Model and Analysis

A schematic diagram of the proposed SMF28-HCF-SMF28 fiber structure is shown in Fig. 1(a). A microscope image is also presented in Fig. 1(b) to illustrate the splice condition at the transition region between the SMF28 and HCF. When light is transmitted from the SMF28 to the HCF, the light energy within the SMF28 core is not fully guided mode within the HCF since the diameter of the air core (~30 μm) of the HCF is larger than that of the SMF28 (~8.2 μm) and the refractive index of the air core is much smaller than that of the silica cladding of the HCF. Light that reaches the silica cladding of the HCF propagates within the cladding, given that the cladding is surrounded an air with a lower refractive index. As illustrated in Fig. 1(a), the incident light from the SMF28 will be reflected at both the interface between the inner air/cladding and outer air/cladding, resulting in multiple beam interferences within the HCF. After experiencing the multiple beam interference in the HCF cavity light will ultimately be transmitted to the output SMF28. Since the fiber has a symmetric cylindrical structure, the light interference and transmission are illustrated in Fig. 1(a) but only for the top half of the structure for the sake of clarity.

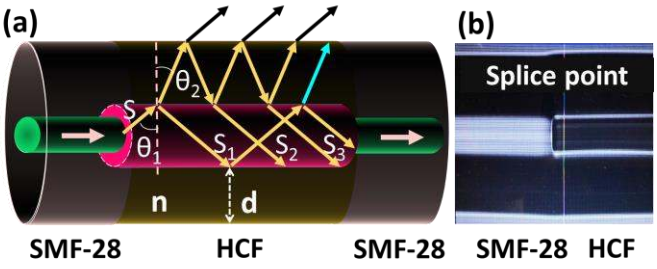

FIG. 1. (a) A schematic diagram of the proposed SMF28-HCF-SMF28 fiber structure, and (b) a microscope image showing an example of the transition region between the SMF28 and HCF after splicing.

Assuming the input light (S) has an amplitude A with an incident angle θ_1 and a refractive angle θ_2, the HCF cladding thickness is d and the refractive index is n, then the phase difference between the two adjacent reflected light rays inside the air core of the HCF (S_1, S_2, S_3…) is $\delta = \frac{4\pi}{\lambda} ndcos\theta_2$. The complex amplitude of the reflected light S_1, S_2, S_3… can be expressed as

$$r_1 A,\ t_1 t_2 r_2 A e^{i\delta},\ t_1 t_2 r_2^3 A e^{i2\delta}, \cdots\ t_1 t_2 r_2^{2p-3} A e^{i(p-1)\delta}, \cdots$$

where r_1, r_2 are the coefficients of reflection at the interfaces between the inner air/cladding and cladding/outer air respectively which can be calculated by the Fresnel equations:

$$TE\ mode \quad r_1 = \frac{cos\theta_1 - ncos\theta_2}{cos\theta_1 + ncos\theta_2}, r_2 = -r_1 \tag{1}$$

$$TM\ mode \quad r_1 = \frac{cos\theta_2 - ncos\theta_1}{cos\theta_2 + ncos\theta_1}, r_2 = -r_1 \tag{2}$$

t_1, t_2 are the coefficients of refraction at the interface between the inner air/cladding and cladding/outer air respectively.

$$t_1 = t_2 \tag{3}$$

$$t_1^2 + r_1^2 = 1 \tag{4}$$

If there are p reflected light rays, where $p = \frac{L}{2dtan\theta_2}$, L is the length of the HCF fiber, then the amplitude of reflected light can thus be expressed as:

$$A_r = r_1 A + t_1 t_2 r_2 A e^{i\delta} + t_1 t_2 r_2^3 A e^{i2\delta} + \cdots + t_1 t_2 r_2^{2p-3} A e^{i(p-1)\delta} + \cdots \tag{5}$$

The intensity of light reflected by the HCF cladding is hence

$$I_r = |A_r|^2 \tag{6}$$

This article has been accepted for publication in a future issue of this journal, but has not been fully edited. Content may change prior to final publication. Citation information: DOI 10.1109/JLT.2017.2784544, Journal of Lightwave Technology

Simulations based on the above analysis were carried out. In the simulation, we assume the SMF28 has core and cladding refractive indices of 1.452 and 1.449 at a wavelength of 1550 nm respectively and a core diameter of 8.2 μm; the HCF has an air core diameter of 30 μm and cladding diameter of 126 μm with the length of 5 mm and only TE mode was considered. The refractive index of the HCF cladding is wavelength dependent,

$$n = \sqrt{1 + \frac{0.6961663\lambda^2}{\lambda^2 - 0.0684043^2} + \frac{0.4079426\lambda^2}{\lambda^2 - 0.1162414^2} + \frac{0.8974794\lambda^2}{\lambda^2 - 9.896161^2}}$$ [29],

where λ is the wavelength in μm, a typical refractive index at the wavelength of 1550 nm is 1.444.

Figure 2 shows the simulated spectral response of the SMF-HCF-SMF fiber structure, based on the analysis above. As one can see from Fig. 2(a), the output spectrum of this structure has multiple high Q transmission dips and a relatively large free spectral range (FSR) of about 23 nm around 1540 nm, making the proposed SMF-HCF-SMF structure advantageous as a very narrow bandwidth optical filter or as a sensor with high accuracy (due to the high Q factor) and a wide working range (due to the large FSR). In practice, the HCF cladding diameter fluctuates very slightly, as a result of the limitations in the manufacturing process, which could have a significant influence on the transmission spectrum of the SMF-HCF-SMF structure. Figure 2(b) shows a simulation result of the spectral response of the structure containing HCF section with random fiber cladding diameter variations of ±10 nm ($d = 48 \pm b \times 0.01$ μm, where b is a random number between 0 and 1). It is clear that the cladding diameter variations have a significant influence on the output spectrum, resulting in a degraded Q factor of 3.15×10^4, which in fact is still relatively high compared to most optical fiber based interferometers, even compared with a typical fiber Bragg grating which has a 3 dB bandwidth of 0.1 nm with a Q factor of 1.55×10^4. Figure 2(c) shows in simulation the relationship between Q and the HCF cladding diameter variation amplitude. It can be seen that the HCF cladding diameter variation has a significant influence on the Q factor of the structure. When the amplitude of the cladding diameter variation increases from 2 nm to 20 nm, the Q factor decreases from 8.13×10^5 to 7.9×10^3. The influence of temperature on the physical properties of an optical fiber manifests itself as both changes of refractive index and changes in fiber dimensions. The values of the changes in each of the properties are further determined by the two fiber material's parameters: the thermal expansion coefficient (TEC) and the thermo-optic coefficient (TOC). For the structure presented here, assuming the HCF has a cladding diameter D, length L and refractive index n, the corresponding changes of these parameters due to a temperature variation (ΔT) can be expressed, respectively, as

$$D_T = D_0 + \alpha \cdot D_0 \cdot \Delta T \quad (7)$$

$$L_T = L_0 + \alpha \cdot L_0 \cdot \Delta T \quad (8)$$

$$n_T = n_0 + \xi \cdot n_0 \cdot \Delta T \quad (9)$$

where α and ξ are the TEC and the TOC, respectively.

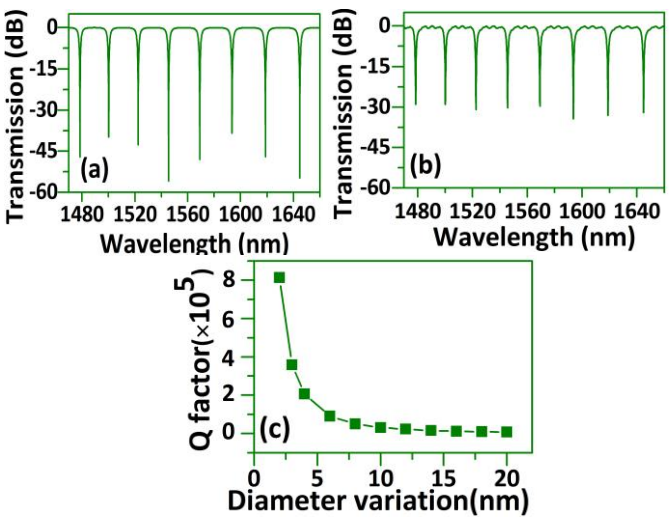

FIG. 2. Simulated spectral response of the SMF-HCF-SMF fiber structure (a) no diameter variation (b) HCF cladding diameter variation amplitude of ±10 nm and (c) Q factor vs. amplitude of HCF cladding diameter variation.

Figure 3 presents the simulation results for the wavelength of one of the transmission dips versus temperature. In the simulation, $\alpha = 5\times10^{-7}$ /°C and $\xi = 8.6\times10^{-6}$ /°C. As the temperature increases, the spectral wavelength red-shifts linearly and monotonically toward the longer wavelengths. The calculated sensitivity is about 25 pm/°C over a wide temperature range from 0 to 900 °C.

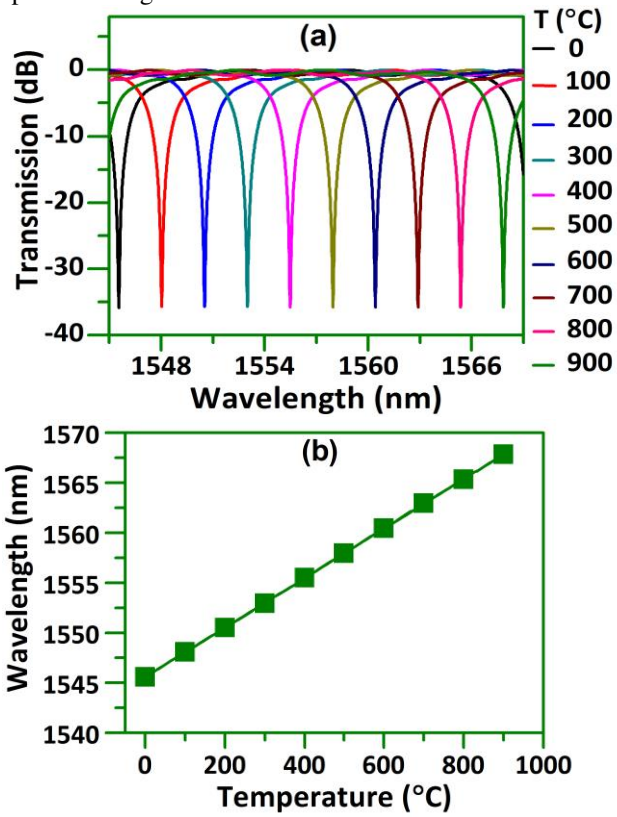

FIG. 3. (a) Simulated transmission responses of the SMF-HCF-SMF fiber structure at different temperatures; and (b) the corresponding spectral shift of a selected transmission dip versus temperature

Experimental investigation of the temperature influence on the HCF based structure has been carried out. Figure 4 shows a

This article has been accepted for publication in a future issue of this journal, but has not been fully edited. Content may change prior to final publication. Citation information: DOI 10.1109/JLT.2017.2784544, Journal of Lightwave Technology

schematic diagram of the experimental setup for temperature/strain measurements. Two ends of SMF-28 are fixed on two manual translation stages and the short section of HCF which is spliced between these two SMF acting as the sensor head is placed straight inside the central heating zone of a ceramic microheater. The temperature of the microheater is controlled by a programmable DC current controller.

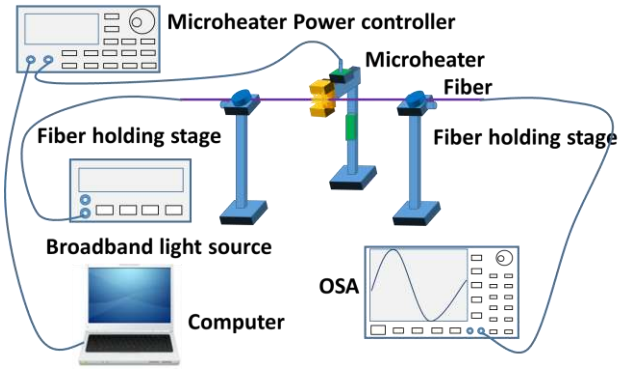

FIG. 4. Schematic diagram of the experimental setup for temperature and strain measurements.

III. Results and Discussion

Figure 5(a) shows the experimentally measured transmission spectral responses of the proposed structures with different lengths of HCF. As one can see from the figure, a range of sharp transmission dips are observed over the wavelength range from 1493 to 1593 nm, which agrees well with our above simulation results. As the length of the HCF increases from 3.5 mm to 8.5 mm, the transmission loss increases, the estimated Q factor values for the experimentally recorded spectral responses (for dip 2) are about 7.3×10^3, 3.3×10^4, 1.3×10^4 and 1.1×10^4, respectively, demonstrating that high Q factors can be achieved experimentally. The measured FSR around the wavelength of 1540 nm range is circa 23 nm, which matches very well with the simulation result. Figure 5(a) also shows that the minimum transmission loss of the structure is about 5 dB corresponding to a sample with a HCF length of 3.5 mm. The loss is possibly due to the following two factors: 1) the light absorption/ scattering at the interface between HCF cladding and air; 2) the SMF fiber has much smaller diameter (8.2 μm) compared to that of HCF air core (30 μm), so that not all the power transmitted in the HCF air core will be coupled to the output SMF. The loss due to the above factors can be reduced by replacing the output SMF with a larger core diameter multimode fiber (MMF), which has been verified by our additional experiment, where the transmission loss was reduced by about 2.5 dB as shown in Fig. 5(b) by replacing SMF28 with MMF with a core diameter of 62.5 μm.

It should be noted also that the wavelengths of the spectral dips remain almost unchanged for the structures with different lengths of HCF, which indicates that the spectral dip wavelength of the transmission is independent of the HCF length. This is due to the fact that the interference wavelength dip is caused by the multiple beam interferences taking place within the hollow core of the HCF. The unique property makes the fabrication of this device more repeatable.

The temperature dependence of the HCF based structure has been experimentally investigated. In our experiments, a sensor with a length of circa 3.5 mm of HCF is chosen for the test. Since the microheater used in our setup has a full length of heating zone of 19 mm, it is reasonable to assume that this microheater can provide a uniform temperature distribution over the whole length of the 3.5 mm HCF section.

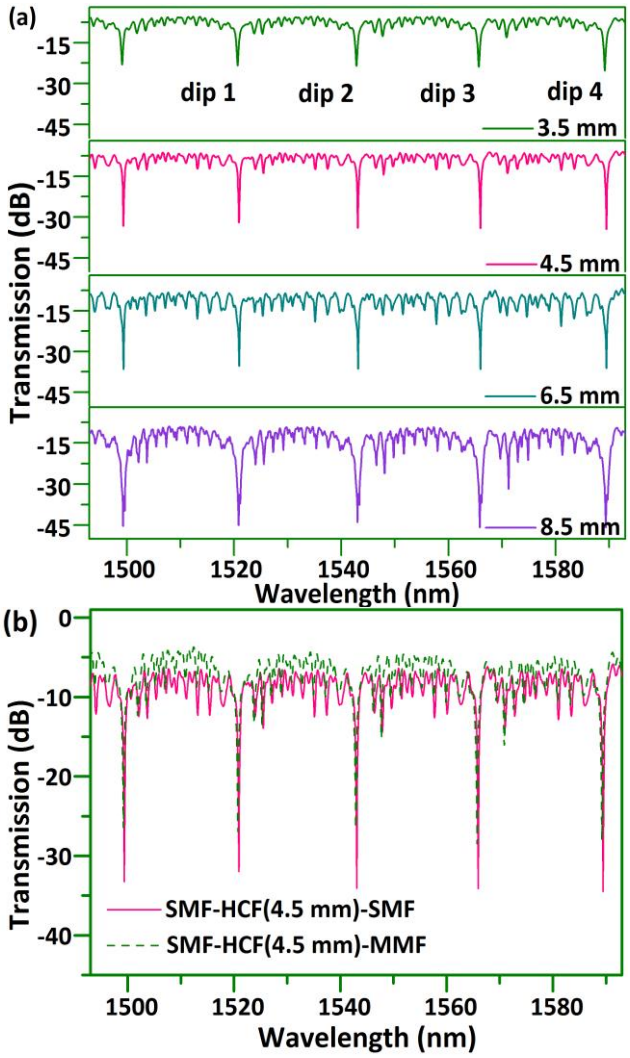

FIG. 5. Measured transmission spectra for HCF based fiber structure with (a) different lengths of HCF and (b) different output fiber types of SMF and MMF.

As in initial set of tests, the sensor stability at high temperatures is monitored over a one hour period as shown in Fig. 6(a). The sensor demonstrates a very good stability when it is exposed to constant temperatures of 500 °C and 638 °C. When the temperature is further increased to a constant value of 777 °C, the optical spectrum undergoes a blue shift of circa 0.56 nm over 60 minutes. Further increases in the temperature to constant values of 900 °C and 1005 ℃, result in the blue shift increase with time becoming more significant, which indicates the sensor's stability deteriorates with the long term exposure to higher temperatures, above 800 °C. This problem can be solved by introducing an annealing process which helps to eliminate the residual stress and thermal memory existing in the fiber structure [11, 30]. As shown in Fig. 6(a), after one cycle of a 65

This article has been accepted for publication in a future issue of this journal, but has not been fully edited. Content may change prior to final publication. Citation information: DOI 10.1109/JLT.2017.2784544, Journal of Lightwave Technology

hour annealing process at 900 °C and 1005 °C respectively, sensor stability has been significantly improved. Figure 6(b) shows a standard deviation plot for the spectral dip's variations during one hour period at different temperatures before and after the annealing process, which clearly demonstrates that the sensor has a significantly improved stability after 65 hours of annealing. It is also acknowledged that the observed small variations in the temperature dependencies at higher temperatures could possibly be contributed by the microheater itself as a result of the perturbations caused by the local airflow or small fluctuations in the output of the DC current controller driving the microheater.

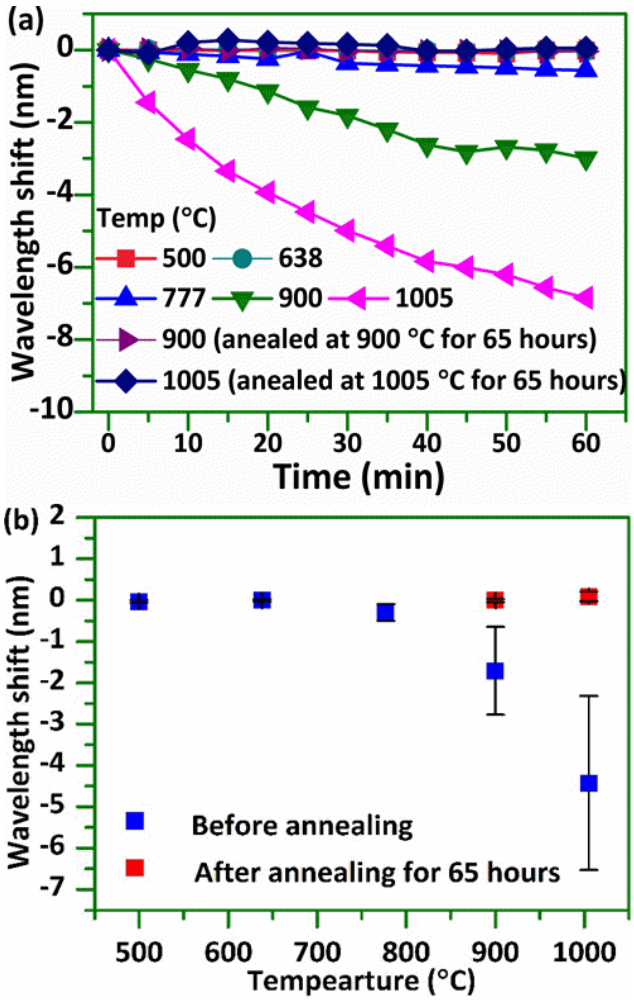

FIG. 6. (a) HCF based sensor (HCF=3.5 mm) stability test and (b) the corresponding standard deviation plot in one hour period before and after the annealing process at different temperatures.

Following the temperature stability tests above, the temperature sensing performance for the sensor has been investigated. Initially this took place without an annealing process. As can be seen from Fig. 7(a), spectral dip 3 (marked in Fig. 5(a)) moves monotonically towards longer wavelengths as the temperature increases from room temperature to 500 °C. Each of the associated spectral dips corresponding to longer wavelengths display slightly improved temperature sensitivity.

The main graph in Fig. 7(b) shows the wavelength shift versus temperature for heating and cooling cycles for the same sensor which underwent three different annealing cases in sequence (no annealing (NA), then annealed at 900 °C (A900) and then subsequently annealed at 1005 °C (A1005)). For each annealing case, including no annealing, the sensor was characterized in terms of wavelength shift as a function of temperature over a range from room temperature up to a defined limit, as shown in Fig. 7(b). The sensor was also characterized for a decreasing temperature, from the upper limit of a range, back down to room temperature. The NA case used a measurement range from room temperature to 503 °C, as without annealing operation beyond circa 500 °C is not reliable. For the cases where the sensor was annealed at 900 °C and annealed at 1005 °C, the temperature range was from room temperature up to 899 °C, and up to 998 °C, respectively.

The results show that, for all the three different annealing cases, the measured wavelength shifts for the heating cycle match very well with those of the cooling cycle, indicating that this structure has very good repeatability for temperature measurement, with negligible evidence of hysteresis. From Fig. 7 (b) we can also see that, the temperature sensitivities are almost the same for all the sensors even after three different annealing processes.

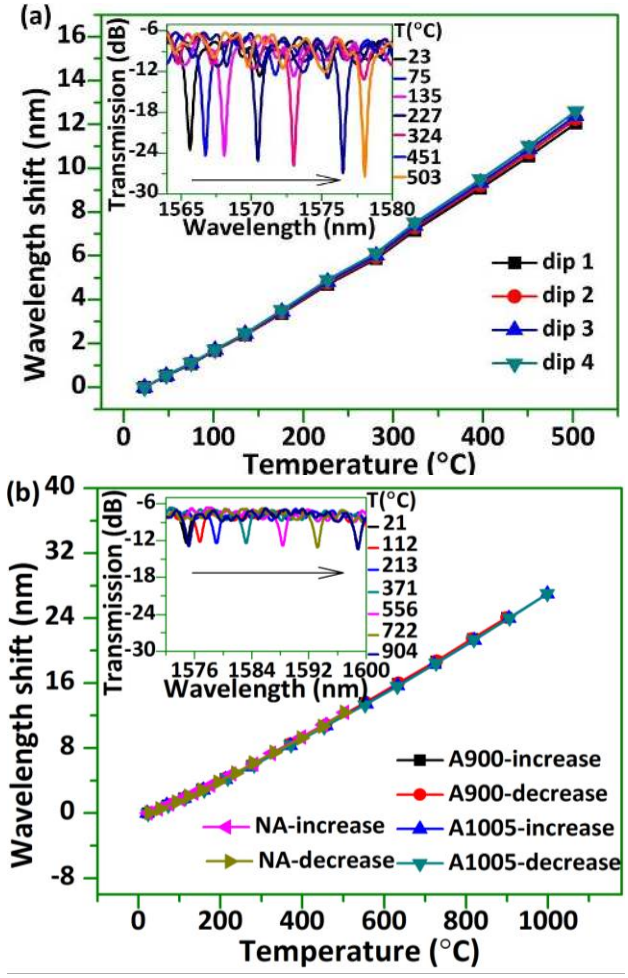

FIG. 7. Wavelength shift versus temperature for HCF based sensor (HCF=3.5 mm): (a) dependencies for different dips within transmission spectrum for the sensor with no pre-annealing process and an example in the inset of the spectral response for dip 3 at different temperatures; (b) dependencies for the same transmission dip for all three different annealing processes and in the inset an example of spectral response at a selected dip for the sensor after annealing at 1005 °C for 65 hours.

This article has been accepted for publication in a future issue of this journal, but has not been fully edited. Content may change prior to final publication. Citation information: DOI 10.1109/JLT.2017.2784544, Journal of Lightwave Technology

The maximum temperature sensitivity of 33.4 pm/°C is achieved at the temperature around 1000 °C for the sensor after being annealed at 1005 °C, which is over two times higher than many temperature sensors reported recently [9,13,17]. It is noted that the measured maximum sensitivity is larger than our theoretically calculated temperature sensitivity of 25 pm/°C, this is possibly because the TOC (ξ) of the HCF cladding is temperature dependent and it has a higher value of ξ at high temperatures. Due to the large FSR, the annealed sensor can effectively measure temperature in very wide temperature range from room temperature to 1000 °C with excellent stability. The inset figure in Fig. 7(b) gives a spectral response vs. temperature for the sensor after annealed at 1005 °C for 65 hours, which shows similar wavelength shifting trend but with a reduced Q factor (5.1×10^3) and extinction ratio.

The influence of strain applied to the structure on its performance as a temperature sensor has also been investigated. In our experiment, the sensor which underwent annealing at 1005 °C is chosen for the strain test at different temperatures. For the sake of brevity, we only present the spectral responses to strain at room temperature and at 503 °C as shown in Fig. 8. It can be seen that wavelength shifts linearly with strain, and the strain sensitivities at both temperatures are almost the same, (0.64 pm/με at 503 °C and 0.66 pm/με at room temperature), indicating that the structure's strain sensitivity is temperature independent over a wide temperature range.

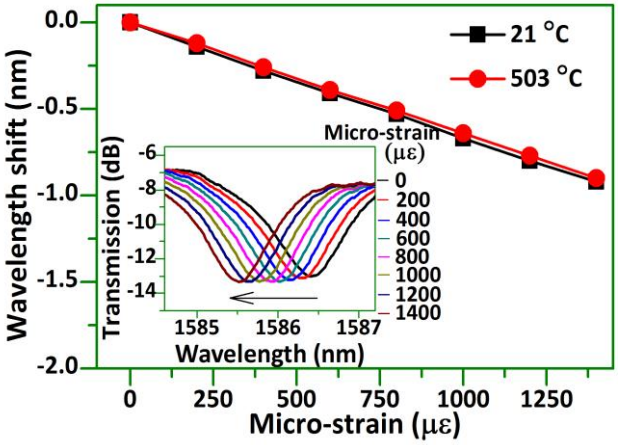

FIG. 8. Spectral wavelength shift versus applied strain at 21 °C and 503 °C, and spectral responses to various strains at 503 °C for the sensor annealed at 1005 °C for 65 hours.

The influence of the HCF length on both the temperature and strain sensitivities of the sensor has also been studied and the results are shown in Fig. 9. Due to the limited heating length of the micro-heater it wasn't suitable for this experiment and so the influence of HCF length on temperature sensitivity was analyzed at lower temperatures by placing the fiber structure on a hotplate. It is clear from the figure that the HCF length has a limited influence on the temperature sensitivity. However, a greater length somehow shows a lower strain sensitivity of 0.46 pm/με, which is lower than many other fiber structures such as FBG (1.2 pm/με) [31], long-period fiber-grating (7.6 pm/με) [32] and hollow-core photonic crystal fiber (0.96 pm/με) [33]. Usually, a strain change will introduce the variation of fiber length and hence the optical length change, resulting spectral wavelength shifts. However, the spectral position of the interference dips does not change with fiber length in our case.

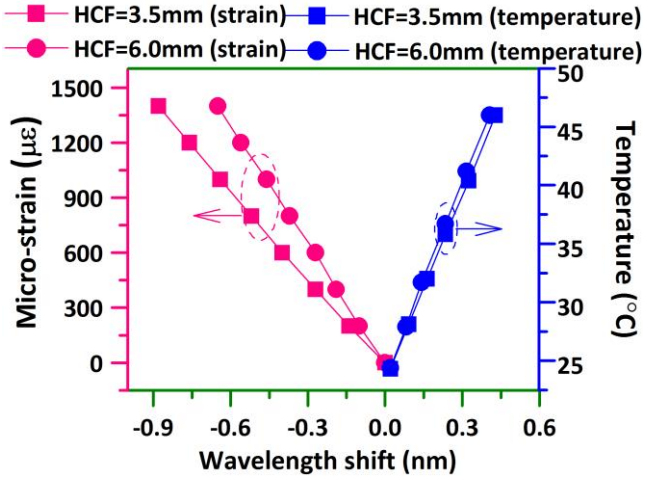

Fig. 9. Influence of the HCF length on temperature and strain sensitivities of the proposed sensor.

IV. Conclusion

In conclusion, a high temperature sensor based on a HCF based interferometer is proposed and investigated both theoretically and experimentally. It is found that the interferometer's transmission spectrum contains dips with a very high spectral extinction ratio and high Q factors due to multiple beam interference introduced by the hollow fiber cladding, but theoretical analysis shows that minor variations of the HCF cladding diameter may result in a significant decrease in the Q factor. Hence, accurate control of the fiber cladding diameter is critical to achieve high Q transmission dips. Experimentally, a range of periodic transmission dips with large spectral extinction ratio (~ 26 dB), large FSR (~ 23 nm) and high Q factor (3.3×10^4) were demonstrated based on the proposed fiber structure, which agrees very well with the simulation results. Experimental results also show that the length of HCF has influence on the spectral Q factor and transmission power, but it has no effects on position of the periodic transmission dips. The proposed HCF based structure has a maximum temperature sensitivity of 33.4 pm/°C with good stability at 1005 °C after proper annealing process. In addition, the structure is relatively insensitive to strain with a sensitivity of circa 0.46 pm/με, which gives the sensor great potential for high temperature sensing. Due to the high Q factor of the structure, it has potential application as high accuracy bio-chemical sensor assuming proper functionalizing inner/outer surface of the HCF. It has many other advantages such as a simple configuration, ease of fabrication, low cost, and also excellent stability and repeatability.

V. References

[1] D. Liu, A. K. Mallik, J. Yuan, C. Yu, G. Farrell, Y. Semenova, and Q. Wu, "High sensitivity refractive index sensor based on a tapered small core single-mode fiber structure," Opt. Lett., vol. 40, pp. 4166–4169, 2015.

[2] W. Yu, T. Lang, J. Bian, W. Kong, "Label-free fiber optic biosensor based on thin-core modal interferometer," Sens. Actual. B: Chem., vol. 228, pp. 322–329, 2016.

[3] D. Liu, Wei Han, A. K. Mallik, J. Yuan, C. Yu, G. Farrell, Y. Semenova, and Q. Wu, "High sensitivity sol-gel silica coated optical fiber sensor for detection of ammonia in water," Opt. Express, vol. 24, pp. 24179–24187, 2016.

[4] H.N. Li, D.S. Li, G.B. Song, "Recent applications of fiber optic sensors to health monitoring in civil engineering," Eng. Struct., vol. 26, pp. 1647-1657, 2004.

[5] X. Jiang, K. Wang, J. Li, H. Zhan, Z. Song, G. Che, and G.Lyu, "Optical Sensor of Thermal Gas Flow Based on Fiber Bragg Grating," Sensors, vol. 17, pp. 374, 2017

[6] A. D. Kersey, "Fiber grating sensors", J. Lightwave Technol., vol. 15, pp. 1442-1463, 1997.

[7] B. W. Zhang and M. Kahrizi, "High-Temperature Resistance Fiber Bragg Grating Temperature Sensor Fabrication," IEEE Sens. J., vol. 7, pp. 586–591, 2007.

[8] D. Grobnic, S. J. Mihailov, C. W. Smelser, and H. Ding, "Sapphire fiber Bragg grating sensor made using femtosecond laser radiation for ultrahigh temperature applications," Photonics Technol. Lett., vol. 16, pp. 2505–2507, 2004.

[9] H. Z. Yang, X. G. Qiao, M. Paul, and D. Shyamal, "Thermal regenerated grating operation at temperatures up to 1400°C using new class of multimaterial glass-based photosensitive fiber," Opt. Lett., vol. 39, pp. 6438–6441, 2014.

[10] S. Li-Yang, T. Wang, J. Canning, K. Cook, and T. Hwa-Yaw, "Bulk regeneration of optical fiber Bragg gratings," Appl. Opt., vol. 51, pp. 7165–7169, 2012.

[11] J. E. Antonio-Lopez, Z. S. Eznaveh, P. LiKamWa, A. Schülzgen, and R. Amezcua-Correa, "Multicore fiber sensor for high-temperature applications up to 1000 °C," Opt. Lett., vol. 39, pp. 4309–4312, 2014.

[12] J. Zhu, A. Zhang, T.-H. Xia, S. He, and W. Xue, "Fiber-Optic High-Temperature Sensor Based on Thin-Core Fiber Modal Interferometer," IEEE Sens. J., vol. 10, pp. 1415–1418, 2010.

[13] Y. Liu, S. Qu, and Y. Li, "Single microchannel high-temperature fiber sensor by femtosecond laser-induced water breakdown," Opt. Lett., vol. 38, pp. 335–337, 2013.

[14] Y. Zhang, L. Yuan, X. Lan, A. Kaur, J. Huang, and H. Xiao, "High-temperature fiber-optic Fabry-Perot interferometric pressure sensor fabricated by femtosecond laser," Opt. Lett., vol. 38, pp. 4609–4612, 2013.

[15] P. Rugeland and W. Margulis, "Revisiting twin-core fiber sensors for high-temperature measurements," Appl. Opt., vol. 51, pp. 6227–6232, 2012.

[16] G. Coviello, V. Finazzi, J. Villatoro, and V. Pruneri, "Thermally Stabilized PCF-Based Sensor for Temperature Measurements up to 1000 °C," Opt. Express, vol. 17, pp. 21551–21559, 2009.

[17] C. Wu, H. Y. Fu, K. K. Qureshi, B. O. Guan, and H. Y. Tam, "High-pressure and high-temperature characteristics of a Fabry–Perot interferometer based on photonic crystal fiber," Opt. Lett., vol. 36, pp. 412–414, 2011.

[18] Born. Max, Wolf. Emil, in Principles of Optics: Electromagnetic Theory of Propagation, Interference and Diffraction of Light (Cambridge University Press, 1999), p. 366.

[19] C. L. Lee, L. H. Lee, H. E. Hwang, and J. M. Hsu, "Highly Sensitive Air-Gap Fiber Fabry–Pérot Interferometers Based on Polymer-Filled Hollow Core Fibers," IEEE Photon. Tech. Lett., vol. 24, pp. 149–151, 2012.

[20] C. L. Lee, H. Y. Ho, J. H. Gu, T. Y. Yeh, and C. H. Tseng, "Dual hollow core fiber-based Fabry–Perot interferometer for measuring the thermo-optic coefficients of liquids," Opt. Lett., vol. 40, pp. 459–462, 2015.

[21] M. S. Ferreira, L. Coelho, K. Schuster, J. Kobelke, J. L. Santos, and O. Frazao, "Fabry–Perot cavity based on a diaphragm-free hollow-core silica tube," Opt. Lett., vol. 36, pp. 4029–4031, 2011.

[22] D. W. Duan, Y. J. Rao, Y. S. Hou, and T. Zhu, "Microbubble based fiber-optic Fabry–Perot interferometer formed by fusion splicing single-mode fibers for strain measurement," Appl. Opt., vol. 51, pp. 1033–1036, 2012.

[23] Y. J. Rao, M. Deng, D. W. Duan, X. C. Yang, T. Zhu, and G. H. Cheng, "Micro Fabry-Perot interferometers in silica fibers machined by femtosecond laser," Opt. Express, vol. 15, pp. 14123–14128, 2007.

[24] T. Wei, Y. K. Han, H. L. Tsai, and H. Xiao, "Miniaturized fiber inline Fabry-Perot interferometer fabricated with a femtosecond laser," Opt. Lett., vol. 33, pp. 536–538, 2008.

[25] A. M. Zheltikov, "Ray-optic analysis of the (bio)sensing ability of ring-cladding hollow waveguides," Appl. Opt., vol. 47, pp. 474–479, 2008.

[26] R. Gao, Y. Jiang, and Y. Zhao, "Magnetic field sensor based on anti-resonant reflecting guidance in the magnetic gel-coated hollow core fiber," Opt. Lett., vol. 39, pp. 6293–6296, 2014.

[27] R. Gao, D. Lu, J. Cheng, Y. Jiang, L. Jiang, and Z. Qi, "Humidity sensor based on power leakage at resonance wavelengths of a hollow core fiber coated with reduced graphene oxide," Sens. Actuat. Biol. Chem., vol. 222, pp. 618–624, 2016.

[28] R. Gao, D. F. Lu, J. Cheng, Y. Jiang, L. Jiang, and Z. M. Qi, "Optical displacement sensor in a capillary covered hollow core fiber based on anti-resonant reflecting guidance," IEEE J. Sel. Top. Quantum Electron., vol. 23, pp. 5600106, 2017.

[29] I. H. Malitson, "Interspecimen comparison of the refractive index of fused silica", J. Opt. Soc. Am., vol. 55, pp. 1205–1209, 1965.

[30] D. Grobnic, C. W. Smelser, S. J. Mihailov, and R. B. Walker, "Long-term thermal stability tests at 1000 degree C of silica fiber Bragg grating made with ultrafast laser radiation," Meas. Sci. Technol., vol. 17, pp. 1009–1013, 2006.

[31] A. Othonos, "Fiber Bragg gratings," Rev Sci Instrum., vol. 68, pp. 4309, 1997.

[32] Y. P. Wang, D. N. Wang, W. Jin, Y. J. Rao, and G. D. Peng, "Asymmetric long period fiber gratings fabricated by use of CO_2 laser to carve periodic grooves on the optical fiber," Appl. Phys. Lett., vol. 89, pp. 151105, 2006.

[33] S. H. Aref, R. Amezcua-Correa, J. P. Carvalho, O. Frazão, P. Caldas, J. L. Santos, F. M. Araújo, H. Latifi, F. Farahi, L. A. Ferreira, and J. C. Knight, "Modal interferometer based on hollow-core photonic crystal fiber for strain and temperature measurement," Opt. Express, vol. 17, pp. 18669–18675, 2009.